

FRAGMENTATION OF OXYGEN NUCLEUS AS A FUNCTION OF ITS EXCITATION DEGREE IN COLLISIONS WITH PROTONS AT A MOMENTUM OF $3.25A$ GeV/ c

KH.K. OLIMOV, K.OLIMOV, S.L. LUTPULLAEV, A.K. OLIMOV,
A.A. YULDASHEV, E.I. ISMATOV¹

UDC 539
©2007

Physical and Technical Institute, Scientific Production Association "Physics–Sun",
Uzbek Academy of Sciences

(2b, G. Mavlyanov Str., Tashkent 700084, Uzbekistan; e-mail: olimov@uzsci.net),

¹Aktobe State Pedagogical University
(Aktobe, Kazakhstan)

New experimental data concerning the dependences of the average multiplicities of light ($A \leq 3$) fragments and ^4He nuclei, as well as the average kinetic energy of few-nucleon fragments ($A = 1 \div 3$), on the amplitude of 4-momentum transferred by the target proton to the oxygen nucleus in ^{16}O -collisions at a momentum of $3.25A$ GeV/ c have been obtained under the conditions of 4π -geometry. Experimental data concerning the probabilities of the formation of light fragments, ^4He nuclei, and multicharged fragments in inelastic ^{16}O -collisions, as well as their dependences on the amplitude of 4-momentum transferred by the target proton, have been obtained for the first time. A comprehensive comparison of the data obtained with the results of calculations made in the framework of the cascade-fragmentation evaporation model (CFEM) was made.

the majority of experiments dealing with the nucleus fragmentation were carried out for heavy nuclei, so that the restoration of the structure of final states became practically impossible. If a large number of fragments are formed, the exclusive measurements are needed in order to determine the degree of fragmentation and its interrelation with the formation of new particles. Such experiments are easier to be carried out in the case of light projectile nuclei [7]. Third, the majority of experiments devoted to hadron–nucleus and nucleus–nucleus collisions are electronic, where the formation of fragments is studied within narrow solid angles, so that, as a consequence, a substantial portion of new fragments – mainly, light ones – are not registered, which considerably reduces the scope of the extracted helpful information concerning the fragmentation process dynamics. Since light fragments are predominantly formed at the very initial stage of the interaction between nuclei, they include a straightforward information on the reaction dynamics.

1. Introduction

One of the fundamental problems of modern nuclear physics is the identification of fragmentation mechanisms for nuclei at their interaction with hadrons and other nuclei. It has been found experimentally [1] that, at intermediate energies (several gigaelectronvolts per nucleon), the fragmentation makes a dominant contribution to the multiplicity of secondary particles. Although a large number of experimental and theoretical works were devoted to the research of fragmentation processes, there is still no comprehensive understanding of fragmentation mechanisms, so that the available models provide only a partial description of this phenomenon [2, 3].

Difficulties in the analysis of experimental data are associated, first, with the fact that the fragmentation process is a combination of several mechanisms, whose roles change depending on the collision energy [3], masses of colliding nuclei [4, 5], and, which is not less important, the structure of the fragmenting nucleus [6]. Second,

This work continues the cycle of researches dealing with the fragmentation of oxygen nuclei at their interaction with protons with a momentum of $3.25A$ GeV/ c and is devoted to the study of the fragment formation as a function of the 4-momentum of the target proton, transferred to the oxygen nucleus. We emphasize that our previous works [8–12] contain data on the multiplicities of various fragments and particle types, isotopic composition of the fragments, topological cross-sections of final states, and characteristics of α -particles and light fragments (^1H , ^2H , ^3H , and ^3He), as well as the cross-sections of the formation of short-lived nuclei, when oxygen nuclei disintegrate into multicharged fragments. However, a detailed analysis of the process of oxygen nuclei fragmentation and the dependence of the

latter on the magnitude of 4-momentum $\Delta = (-t)^{1/2}$ transferred to the fragmenting nucleus by the target proton – or, in other words, on the degree of oxygen nucleus excitation – has not been carried out yet. Such an analysis is both interesting and actual, because it would allow one to retrace the degree and the character of the fragmenting nucleus destruction at changing over from peripheral collisions to central ones and to study how the distributions of probabilities, which describe the formation of various fragments, depend on Δ .

Experimental data were measured making use of a 1-m hydrogen bubble chamber at the LHE of the JINR (Dubna, Russia); targets were irradiated by relativistic ^{16}O nuclei generated by a synchrotron. The results of this work were obtained on the basis of the analysis of 11068 measured ^{16}O -events with a momentum of $3.25A$ GeV/ c . The homogeneity of the target and the low density of the working liquid in the chamber allowed the charges of all secondary fragments to be identified unambiguously and their momenta to be measured with a high accuracy. Single- and double-charged fragments with the projections of their track lengths in the working volume of the chamber exceeding $L = 35$ cm were taken for consideration. Provided such a selection, the average relative determination error of momenta did not exceed 3.5% for all fragments. While determining the fragment multiplicities, the corrections for a loss of fragments owing to their interaction with the working liquid in the chamber within the length $L = 35$ cm were made. For the fragments with charges $3 \leq z \leq 8$, such a restriction on the length of their tracks was not introduced, because the identification of their masses was not carried out. We emphasize that no events, where the total charge of multicharged fragments, each with $z \geq 2$, would exceed the charge of fragmenting oxygen nucleus, have been registered within the whole body of experimental results.

Positive single-charged particles with the momenta p from the intervals $1.75 \div 4.75$, $4.75 \div 7.75$, and ≥ 7.75 GeV/ c were considered as proton-fragments, deuterium nuclei, and tritium ones, respectively. Such a selection by the momentum interval allows the isotopes of single-charged fragments to be identified with a probability not less than 96%. Double-charged fragments with the momentum $p < 10.75$ GeV/ c were regarded as ^3He nuclei, and those with the momentum $p > 10.75$ GeV/ c as ^4He ones. In this case, the admixtures of ^3He and ^6He nuclei among ^4He nuclei did not exceed 4 or 0.5%, respectively. Only the completely measured events, the statistical sample of which comprised 8712 ^{16}O -events, were taken into account. Among them, 4828 events containing an identified recoil proton with

the momentum from the interval $p = 0.1 \div 1.5$ GeV/ c have been selected for the further analysis. Elastic events, whose fraction amounts to approximately 50% of two-beam events with one recoil proton and one eightfold-charged fragment, have been excluded at that from the further consideration. The choice of the lower limit for the momentum interval of recoil protons was associated with the registration threshold for slow protons in the hydrogen bubble chamber. On the other hand, the interval was confined from above by the circumstance that the visual resolution of protons and π^\pm -mesons becomes problematic if their momenta p exceed 1.5 GeV/ c . Technical features of the experiment were illustrated in more details in works [13, 14]. The amplitude of the 4-momentum of the proton-target was calculated from the measured momentum of the recoil proton. The momentum interval of recoil protons $p = 0.1 \div 1.5$ GeV/ c approximately corresponds to the interval $\Delta = (-t)^{1/2} = 0.1 \div 1.25$ GeV/ c .

For the physical interpretation of experimental data to be more adequate, a comprehensive comparison was done between them and the results predicted in the framework of the CFEM, which was developed for proton–nucleus interactions at intermediate energies [15]. Note that the CFEM is one of the most developed models, where the multistep character of nucleus fragmentation processes at high energies is made allowance for. In the CFEM framework, the process of interaction is described as that running through several stages. The first stage is the initial stage of the intranuclear cascade, in which an incident proton provokes a cascade of consecutive NN- and πN interactions in the nucleus. The fast particles, which have been generated at that, escape from the nucleus, while the slow ones become captured by the latter. This stage ends by the formation of an excited remnant nucleus. The second stage is the stage, during which the thermalized remnant nucleus decays into a lot of fragments. This process can run, if the excitation energy is high enough. The calculations testify that, owing to an enhanced stability of light nuclei with respect to such a decay, the mechanism of multifragmentation should manifest itself rather weakly in the reaction concerned. The third, final stage includes the deexcitation of excited hot nuclei and the formation of final fragments. This process can run through either the “evaporation” or Fermi decay mechanisms. It should be noted that the “evaporation” mechanism has not been taken into account in this model while examining the formation of light fragments. Instead, the model makes allowance for the contributions of decays of unstable

nuclei ${}^5\text{He}$, ${}^5\text{Li}$, ${}^8\text{Be}$, and ${}^9\text{B}$ to the final states. In this work, we simulated more than 22000 collision events. The procedure applied for processing the results of calculations and the experimental data was the same.

2. Experimental Results and Their Discussion

In Fig. 1, the dependence of average multiplicities of proton-fragments (hereinafter, protons) on the transferred momentum Δ is displayed. It is evident that the average experimental multiplicity of protons grows as Δ increases. The spectrum of the average proton multiplicity can be split into 2 sections: $\Delta < 0.25$ GeV/c and $\Delta > 0.25$ GeV/c. In the first section, the proton multiplicity grows quickly from a value of 0.11 ± 0.02 at $\Delta = 0.125$ GeV/c to a value of 0.59 ± 0.05 at $\Delta = 0.225$ GeV/c. A small magnitude of the average multiplicity of protons in this section is associated with the peripheral character of ${}^{16}\text{O}$ -collisions. In the other section, at $\Delta > 0.25$ GeV/c, the growth of proton multiplicity considerably slows down, but continues up to the final values of the transferred 4-momentum, by achieving a value of 1.75. In so doing, the multiplicity of protons calculated in the framework of the CFEM remains approximately constant – within the statistical error limits – in the section $\Delta < 0.25$ GeV/c, amounting to 0.75 ± 0.05 on average. It is evident that the model essentially overestimates the multiplicity of protons in the first section. The corresponding analysis demonstrated that this fact is associated with the neglect – in the model – of contributions made by the processes of diffraction decay of oxygen nuclei at peripheral interactions; such as decays into an α -particle and a ${}^{12}\text{C}$ nucleus, four α -particles, a ${}^2\text{H}$ and a ${}^{14}\text{N}$ nucleus, and so on. The overestimation of the proton multiplicity also stems from the overestimation of intranuclear cascade processes by the model at low Δ . In the section $\Delta > 0.25$ GeV/c, the calculation results given by the CFEM for proton multiplicities are in satisfactory agreement with the corresponding experimental values.

In Fig. 2, the dependences of the average multiplicities of ${}^2\text{H}$, ${}^3\text{H}$, ${}^3\text{He}$, and ${}^4\text{He}$ nuclei on Δ are depicted. Panels *a*, *b*, and *c* demonstrate that the experimental multiplicities of light nuclei ${}^2\text{H}$, ${}^3\text{H}$, and ${}^3\text{He}$ grow, in whole, with increase in Δ . It is evident that the model considerably underestimates the multiplicity of deuterons in the interval $\Delta > 0.2$ GeV/c and tritium nuclei in the interval $\Delta > 0.6$ GeV/c, except for a narrow

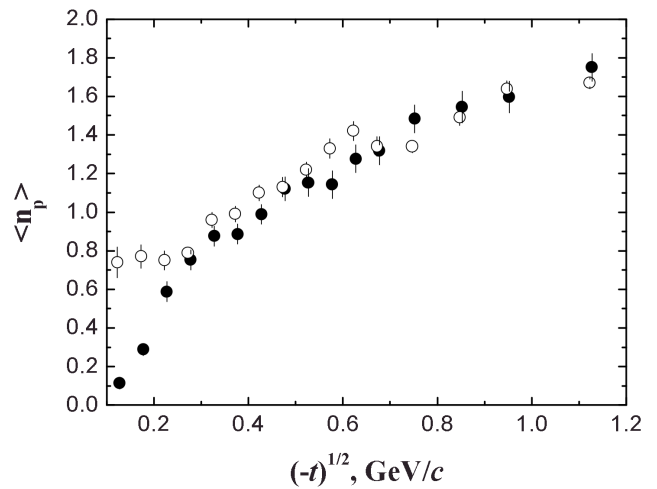


Fig. 1. Dependences of the average multiplicity of proton-fragments on the transferred 4-momentum Δ : experimental data (\bullet) and the results of CFEM calculations (\circ)

section including low Δ -values, where the model gives the results that are overestimated in comparison with experimental multiplicities. From Fig. 2, *c*, one can see that the experimental multiplicity of ${}^3\text{He}$ nuclei behaves – within the statistical error limits – similarly to the average multiplicity of tritium nuclei. Nevertheless, the model reproduces rather well the whole experimental dependence of the average multiplicity of ${}^3\text{He}$ nuclei on Δ .

Figure 2, *d* demonstrates that the experimental dependence of the average multiplicity of ${}^4\text{He}$ nuclei on Δ has a nonmonotonous character. In particular, a drastic growth is observed in the interval $\Delta \approx 0.13 \div 0.23$ GeV/c. Then, this quantity remains practically constant in a wide interval $\Delta = 0.3 \div 0.7$ GeV/c amounting to 0.54 ± 0.06 on the average. Further, in the range $\Delta > 0.7$ GeV/c, the experimental multiplicity of ${}^4\text{He}$ nuclei demonstrates a weak, in whole, growth. It is evident from Fig. 2, *d* that the results of model calculations considerably differ from experimental data. A substantial excess of experimental values for the multiplicity of ${}^4\text{He}$ nuclei over the results of model calculations can be explained by the circumstance that the experimental cross-sections for the formation of two, three, and four double-charged fragments, the overwhelming portion of which (approximately 80%) is constituted by ${}^4\text{He}$ nuclei, are more than twice larger than the corresponding cross-sections calculated in the framework of the CFEM [11].

Consider the dependences of the average kinetic energy $\langle T \rangle$ on Δ for few-nucleon fragments ($A = 1, 2, 3$)

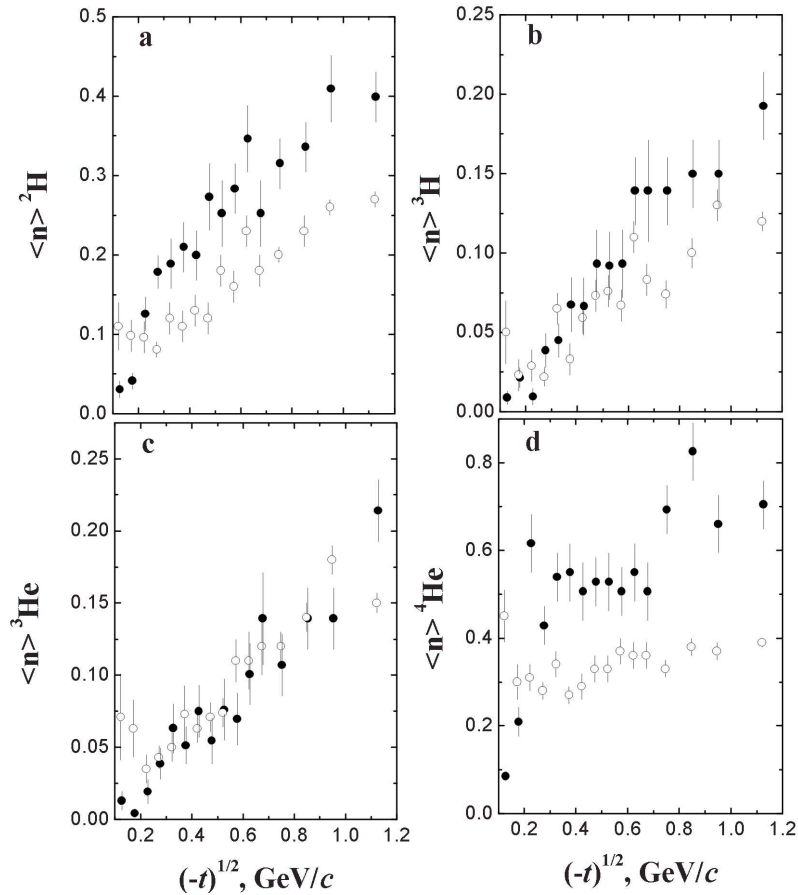


Fig. 2. Dependences of the average multiplicities of ^2H (a), ^3H (b), ^3He (c), and ^4He (d) nuclei on Δ : experimental data (\bullet) and the results of CFEM calculations (\circ)

in the rest system of the oxygen nucleus (see Fig. 3). Panel *a* demonstrates that the average kinetic energy of protons grows in the experiment as Δ increases up to about 0.8 GeV/c. At $\Delta > 0.8$ GeV/c, the $\langle T \rangle$ -spectrum of protons forms a plateau at a level of 94.2 ± 5.2 MeV. The growth of the protons' energy $\langle T \rangle$ in the experiment can be explained by the fact that the increase of the transferred 4-momentum is accompanied by the growth of the kinetic energy of cascade protons knocked out from the oxygen nucleus at the very initial stage of the interaction. To elucidate the origin of such an emergence of the plateau in the spectrum of the average kinetic energy of protons, we examined the average multiplicities of protons and π^\pm -mesons in the plateau region and below. Table 1 quotes the average multiplicities of protons and π^\pm -mesons in the intervals $\Delta = 0.40 \div 0.80$ and $0.80 \div 1.25$ GeV/c. The data presented in the table testify that the average multiplicity of protons in the plateau region is larger by a factor of about 1.35 than the corresponding value for

the interval $\Delta = 0.40 \div 0.80$ GeV/c. The growth of Δ is accompanied by the increase of the multiplicities of slow (with $T < 35$ MeV) and fast (with $T > 35$ MeV) cascade protons. It also follows from Table 1 that the average multiplicity of created π^\pm -mesons in the plateau region $\Delta = 0.80 \div 1.25$ GeV/c is approximately 1.5 times larger than the corresponding multiplicity in the region $\Delta = 0.40 \div 0.80$ GeV/c.

Table 2 demonstrates that the average multiplicities of protons and π^\pm -mesons grow in the plateau region as well. Hence, the attainment of a plateau by the average kinetic energy of protons at $\Delta > 0.8$ GeV/c can be

Table 1. Average multiplicities of protons and π^\pm -mesons in the range $\Delta = 0.4 \div 1.25$ GeV/c

Δ -interval, GeV/c	Average multiplicity of protons			Average multiplicity of π^\pm -mesons
	$T < 35$ MeV	$T > 35$ MeV	All protons	
0.4 – 0.8	0.59 ± 0.02	0.62 ± 0.02	1.22 ± 0.03	0.60 ± 0.02
0.8 – 1.25	0.73 ± 0.03	0.92 ± 0.03	1.65 ± 0.04	0.92 ± 0.03

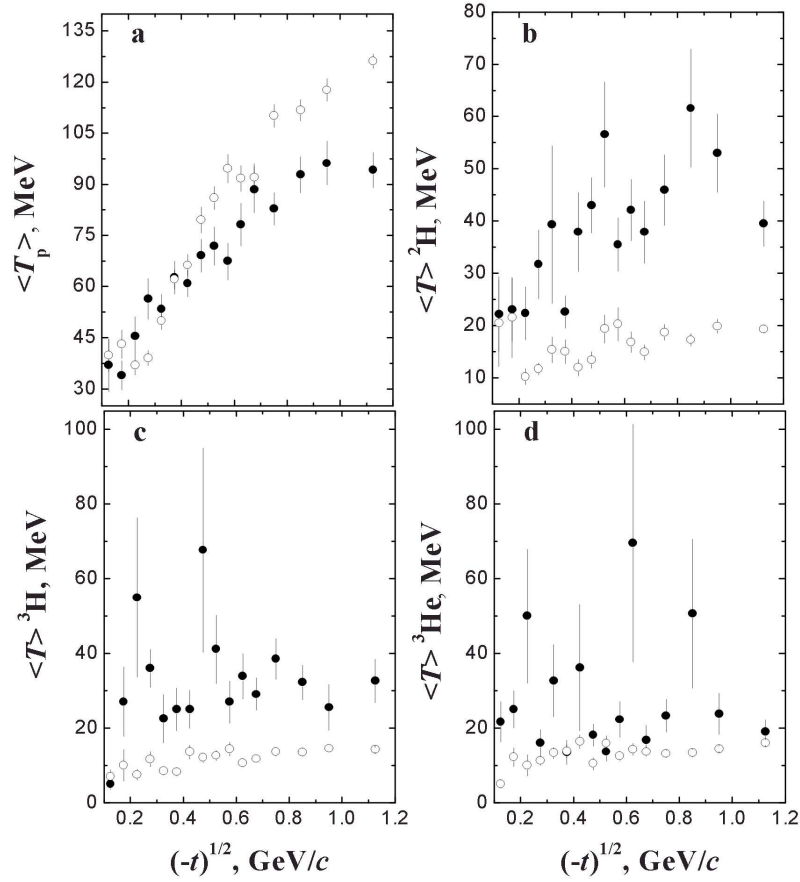


Fig. 3. Dependences of the average kinetic energy of proton-fragments (a), ${}^2\text{H}$ (b), ${}^3\text{H}$ (c), and ${}^3\text{He}$ (d) nuclei in the rest frame of the oxygen nucleus on Δ : experimental data (\bullet) and the results of CFEM calculations (\circ)

explained by the increase of the average multiplicity of both protons and π^\pm -mesons; the creation of the latter consumes an appreciable portion of the energy of ${}^{16}\text{O}$ -collisions, which can ultimately result in stopping the growth of the average kinetic energy per proton. On the other hand, we showed earlier [10, 11] that the coalescence [16] – fusions of fast cascade nucleons with low relative momenta – is responsible for the formation of an appreciable fraction of fast few-nucleon fragments with $A = 2$ and 3. Therefore, the coalescence of some fast cascade protons can lead to the reduction of the average kinetic energy of protons and the formation of the

Table 2. Average multiplicities of protons and π^\pm -mesons in the range $\Delta = 0.8 \div 1.25$ GeV/c

Δ -interval, GeV/c	Average multiplicity of protons			Average multiplicity of π^\pm -mesons
	$T < 35$ MeV	$T > 35$ MeV	All protons	
0.8 – 0.9	0.69 ± 0.05	0.84 ± 0.06	1.53 ± 0.08	0.89 ± 0.05
0.9 – 1.0	0.72 ± 0.05	0.89 ± 0.05	1.61 ± 0.08	0.92 ± 0.05
1.0 – 1.2	0.77 ± 0.04	0.97 ± 0.05	1.74 ± 0.06	0.95 ± 0.04

plateau. As is seen from Fig. 3,a, the model satisfactorily describes the spectrum of the average kinetic energy of protons in the interval $\Delta < 0.5$ GeV/c and considerably overestimates this quantity at $\Delta > 0.5$ GeV/c. It is interesting to note that the model calculations predict the increasing behavior for the average kinetic energy of protons in the region $\Delta > 0.8$ GeV/c, where the experimental data attain the plateau.

From Fig. 3,b, it becomes clear that the model gives considerably reduced values for the average kinetic energy of deuterons. Figures 3,c and 3,d also demonstrate that the model concerned underestimates the average kinetic energy of ${}^3\text{H}$ and ${}^3\text{He}$ nuclei.

For more clearness, Table 3 tabulates the experimental and theoretical values for the kinetic energy of ${}^2\text{H}$, ${}^3\text{H}$, and ${}^3\text{He}$ nuclei averaged over the studied Δ -range. It is evident that the average values of the experimental kinetic energies for ${}^2\text{H}$, ${}^3\text{H}$, and ${}^3\text{He}$ fragments exceed the corresponding theoretical results

by a factor more than 2. At the same time, the model overestimates the average kinetic energy of protons.

In Table 4, the experimental and calculation results for the average values of the transverse momentum of light fragments are presented. The tabulated data also demonstrate that the model underestimates the average transverse momenta of ${}^2\text{H}$, ${}^3\text{H}$, and ${}^3\text{He}$ fragments and overestimates this quantity for protons. In work [10], we showed that the CFEM considerably underestimates the yield cross-section for the fast few-nucleon fragments with $A = 2$ and 3, which can be explained, as was indicated above, by the neglect of the coalescence mechanism. Therefore, a significant excess of the experimental multiplicities for ${}^2\text{H}$ and ${}^3\text{H}$ nuclei over the corresponding calculation results obtained in the framework of the CFEM (see Figs. 2, *a* and *b*) can be explained by the availability of an additional mechanism for the formation of relatively fast few-nucleon fragments – coalescence.

Let us examine how the fractions of light fragments ${}^1\text{H}$, ${}^2\text{H}$, ${}^3\text{H}$, and ${}^3\text{He}$ among all light fragments with $A \leq 3$ – or, in other words, the formation probabilities for those fragments – depend on Δ . The corresponding data are listed in Table 5 and plotted in Figs. 4, *a* and *b*. One can see that the overwhelming portion of fragments among all light fragments – both in experiment and in the theory – includes protons. Figures 4, *a* and *b* also demonstrate that the model substantially overestimates the fraction of protons and underestimates that of deuterons. The experimental fractions of ${}^3\text{H}$ and ${}^3\text{He}$ nuclei are identical, within the statistical error limits, in the whole studied interval of Δ , as it might be expected for these mirror nuclei [11]. However, the CFEM model predicts the fraction of ${}^3\text{He}$ nuclei that exceeds slightly the fraction of ${}^3\text{H}$ ones. This result is confirmed by the data in Table 5, where the average fractions of light fragments ${}^1\text{H}$, ${}^2\text{H}$, ${}^3\text{H}$, and ${}^3\text{He}$ among all light fragments with $A \leq 3$ averaged over the interval $\Delta = 0.10 \div 1.25$ GeV/*c* are presented. As is seen from Fig. 4, *a*, the fraction of protons in the experiment first grows from a value of 68.8% at $\Delta \approx 0.1$ GeV/*c* to 81.3% at $\Delta \approx 0.2$ GeV/*c* and then slowly falls down, by reaching 68.8% at $\Delta \approx 1.1$ GeV/*c*. The fractions of ${}^2\text{H}$, ${}^3\text{H}$, and ${}^3\text{He}$ nuclei first, in contrast to protons, fall down to $\Delta \approx 0.2$ GeV/*c*; then the fraction of ${}^2\text{H}$ nuclei continues to diminish slowly, while the fractions of ${}^3\text{H}$ and ${}^3\text{He}$ nuclei slightly grow up to the final value of Δ . Figure 4, *a* and Table 5 make it evident that the model can describe experimental data only at a qualitative level.

Figure 4 (panels *c* and *d*) also exhibits the experimental and theoretical, respectively, Δ -

dependences of the relative probabilities for the formation of fragments with charges $z = 3 \div 7$ relative to the formation of all multicharged fragments with $3 \leq z \leq 7$. One can see that the overwhelming fraction of fragments among all multicharged fragments with $3 \leq z \leq 7$, both in the experiment and in the model, consists of seven- and sixfold-charged fragments, with the fraction of fragments with $z = 7$ exceeding that of sixfold-charged nuclei. Figure 4, *c* demonstrates that the experimental fractions of six- and sevenfold-charged fragments are identical in the interval $\Delta \approx 0.1 \div 0.2$ GeV/*c* within the statistical error limits. Further, in the interval $\Delta \approx 0.2 \div 0.6$ GeV/*c*, the probabilities of the formation of those fragments differ substantially. In the interval $\Delta \approx 0.2 \div 0.4$ GeV/*c*, the probability of the formation of sevenfold-charged fragments increases, while the fraction of sixfold-charged fragments decreases by 13% on average. At the same time, those fractions reveal the inverse behavior in the interval $\Delta \approx 0.4 \div 0.6$ GeV/*c*: the fraction of fragments with charge $z = 7$ decreases, and the fraction of sixfold-charged fragments increases. Such correlations between the formation probabilities for seven- and sixfold-charged fragments, which are observed in the interval $\Delta \approx 0.2 \div 0.6$ GeV/*c*, may probably originate from the baryon charge conservation in the events. The

Table 3. Kinetic energy of ${}^1\text{H}$, ${}^2\text{H}$, ${}^3\text{H}$, and ${}^3\text{He}$ nuclei averaged over the interval $\Delta = 0.1 \div 1.25$ GeV/*c*

Fragment	$\langle T \rangle$, MeV	
	Experiment	CFEM calculations
${}^1\text{H}$	77.3 ± 1.6	105.3 ± 1.1
${}^2\text{H}$	42.7 ± 2.1	18.2 ± 0.5
${}^3\text{H}$	33.7 ± 2.4	13.4 ± 0.4
${}^3\text{He}$	27.9 ± 3.4	14.5 ± 0.3

Table 4. Transverse momenta of ${}^1\text{H}$, ${}^2\text{H}$, ${}^3\text{H}$, and ${}^3\text{He}$ nuclei averaged over the interval $\Delta = 0.1 \div 1.25$ GeV/*c*

Fragment	$\langle P_t \rangle$, MeV	
	Experiment	CFEM calculations
${}^1\text{H}$	241.1 ± 2.9	286.5 ± 1.7
${}^2\text{H}$	242.8 ± 5.8	173.3 ± 2.0
${}^3\text{H}$	227.6 ± 8.3	192.5 ± 3.1
${}^3\text{He}$	235.3 ± 8.8	206.2 ± 2.7

Table 5. Fractions of ${}^1\text{H}$, ${}^2\text{H}$, ${}^3\text{H}$, and ${}^3\text{He}$ fragments among all light fragments with $A \leq 3$ averaged over the interval $\Delta = 0.1 \div 1.25$ GeV/*c*

Fragment	$\langle W \rangle$, %	
	Experiment	CFEM calculations
${}^1\text{H}$	71.7 ± 1.3	76.8 ± 0.6
${}^2\text{H}$	16.5 ± 0.7	11.6 ± 0.2
${}^3\text{H}$	5.9 ± 0.3	5.0 ± 0.2
${}^3\text{He}$	5.9 ± 0.3	6.6 ± 0.2

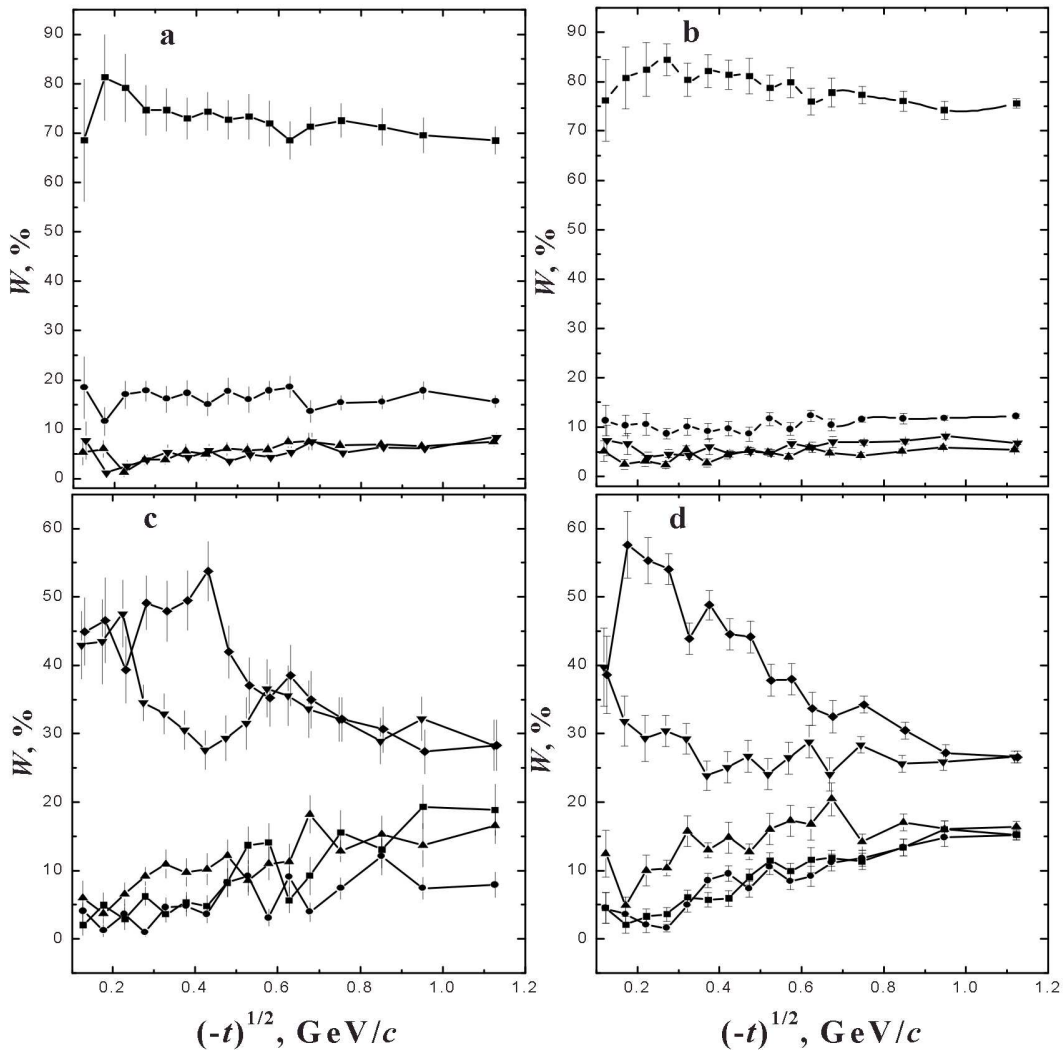


Fig. 4. Dependences of the proton-fragment (■), ${}^2\text{H}$ (◆), ${}^3\text{H}$ (▲), and ${}^3\text{He}$ (▼) nucleus fractions W among all light fragments with $A \leq 3$ on Δ : experimental data (panel *a*) and the results of CFEM calculations (panel *b*). Dependences of the fragment fractions W – among all multicharged fragments with charges from 3 to 7 – on Δ for fragments with charges $z = 3$ (■), 4 (●), 5 (▲), 6 (▼), 7 (◆): experimental data (panel *c*) and the results of CFEM calculations (panel *d*)

growth of the experimental formation probability for sevenfold-charged fragments in the interval $\Delta \approx 0.2 \div 0.4$ GeV/ c can be explained as follows. As was shown in Fig. 1, the interval $\Delta \approx 0.2 \div 0.3$ GeV/ c is the interval of the most intensive growth of the proton multiplicity in the experiment. This fact can be explained by the change from peripheral to nonperipheral collisions as the process of intranuclear cascading develops. The latter promotes the increase of the fraction of those events, in which a proton can be knocked out from an oxygen nucleus, thus forming a residual sevenfold-charged fragment. In this case, a ${}^{14}\text{N}$ nucleus can be formed as a result

of the neutron emission (“evaporation”) from the ${}^{15}\text{N}$ nucleus during its deexcitation. It is of interest to note that the formation probabilities for seven- and sixfold-charged fragments turn out practically identical, within the statistical error limits, in the interval $\Delta > 0.6$ GeV/ c ; they diminish here, in whole, as was expected in the case where the oxygen nucleus destruction degree increases with Δ . As is seen from Fig. 4, *c*, the formation probabilities for the fragments with charges $z = 3 \div 5$ reveal a weak, in whole, increase with the increase of Δ , as was expected for the case of the stronger destruction of fragmenting nucleus. Table 6 testifies that the CFEM

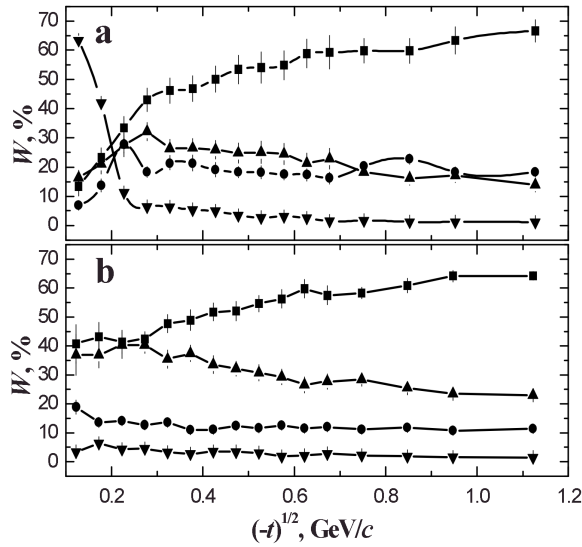


Fig. 5. Dependences of the fragment fractions W – among all multicharged fragments with charges from 1 to 8 – on Δ for light fragments with $A \leq 3$ (■), ${}^4\text{He}$ nuclei (●), multicharged fragments with charges z from 3 to 7 (▲), and fragments with $z = 8$ (▼): experimental data (panel *a*) and the results of CFEM calculations (panel *b*)

overestimates the average fraction of fragments with charges $z = 3 \div 5$ and underestimates this quantity for fragments with $z = 6$ and 7. The table also demonstrates that the largest difference is observed for the average fraction of fourfold-charged fragments, when the model predicts the results that are almost twice as large as the experimental data. As was shown in work [11], the results of theoretical calculations for the scattering cross-section by means of the inelastic interaction through topological channels (4) and (2,4), i.e. through the formation of one fourfold-charged fragment or one double- and one fourfold-charged fragments, exceed the experimental data by a factor more than 2. The results of model calculations, as is seen from Fig. 4,*d*, substantially differ from experimental data. In contrast to the experiment, the model calculations reveal no appreciable correlations between the probabilities of the formation of six- and sevenfold-charged fragments in the interval $\Delta \approx 0.2 \div 0.6$ GeV/*c*. In the model, the formation probabilities for fragments with charges $z = 3 \div 5$ become practically identical, within the statistical error limits, in the interval $\Delta > 0.95$ GeV/*c*, whereas they are notably different in the experiment. But, in whole, the model qualitatively reproduces the reduction of the formation probabilities for six- and sevenfold-charged fragments,

as well as a weak growth of the formation probabilities for fragments with charges $z = 3 \div 5$, with increase in Δ .

In Fig. 5,*a* and 5,*b*, the dependences of the fractions of light fragments with $A \leq 3$, ${}^4\text{He}$ nuclei, multicharged fragments with $3 \leq z \leq 7$, and eightfold-charged fragments among all formed fragments with $1 \leq z \leq 8$ on Δ , obtained in the course of experimental measurements and model calculations, respectively, are depicted. The spectra in Fig. 5,*a* can be split into two sections: $\Delta < 0.23$ GeV/*c* and $\Delta > 0.23$ GeV/*c*. One can see that the experimental fraction of eightfold-charged fragments in the first section considerably exceeds the fraction of light fragments with $A \leq 3$, ${}^4\text{He}$ nuclei, and multicharged fragments with $3 \leq z \leq 7$. In the second section, on the contrary, the fraction of light fragments with $A \leq 3$, ${}^4\text{He}$ nuclei, and multicharged fragments with $3 \leq z \leq 7$ exceeds that of fragments with charge $z = 8$. From Fig. 5,*a*, it is evident that there is a strong reduction of the fraction of eightfold-charged fragments and a strong increase of the fractions of ${}^4\text{He}$ nuclei, light fragments, and multicharged fragments with charges $3 \leq z \leq 7$ in the interval $\Delta \approx 0.13 \div 0.23$ GeV/*c*. The point $\Delta \approx 0.23$ GeV can be designated as a point of the change from the peripheral to nonperipheral ${}^{16}\text{O}p$ -interactions. This change can be seen more precisely in Fig. 6,*a* and 6,*b*, where the dependences of the average number of fragments and their average charge on Δ are presented. One can see that the strongest growth of the average number of fragments occurs at $\Delta \approx 0.23$ GeV/*c*; this growth brings about a strong reduction of the average fragment charge. From Fig. 5,*a*, it also becomes evident that the fraction of ${}^4\text{He}$ nuclei among all the fragments increases at small Δ to reach its maximal value of about 28% at $\Delta \approx 0.23$ GeV/*c*. This growth, as was indicated above, is associated with the processes of diffraction decay of the oxygen nucleus at peripheral interactions. One can see that, in the experiment, the formation probability for α -particles becomes equal, within the statistical error limits, to that for all other fragments

Table 6. Fractions of fragments with charges z from 3 to 7 among all multicharged fragments with $3 \leq z \leq 7$ averaged over the interval $\Delta = 0.1 \div 1.25$ GeV/*c*

Fragment	$\langle W \rangle$, %	
	Experiment	CFEM calculations
$3 \leq z \leq 7$	100	100
$z = 3$	10.2 ± 0.7	11.7 ± 0.4
$z = 4$	5.9 ± 0.5	11.3 ± 0.4
$z = 5$	11.7 ± 0.7	15.5 ± 0.4
$z = 6$	32.8 ± 1.6	26.5 ± 0.5
$z = 7$	39.4 ± 1.6	34.9 ± 0.5

with $3 \leq z \leq 7$. Since the structure of the fragmenting nucleus exerts the greatest influence on the formation of fragments at peripheral interactions, such a high probability of the α -particle formation at small Δ obviously evidences for the availability of the α -cluster structure in the ^{16}O nucleus. The data in Table 7, where the average fractions of light fragments ($A \leq 3$), ^4He nuclei, multicharged ($3 \leq z \leq 7$), and eightfold-charged fragments among all the nuclei with charges $1 \leq z \leq 8$ averaged over the interval $\Delta \approx 0.1 \div 1.25$ GeV/c are listed, confirm this conclusion. This table also demonstrates that the average experimental fractions of ^4He nuclei and multicharged fragments practically coincide within the statistical error limits. Further, in the interval $\Delta \approx 0.23 \div 0.28$ GeV/c, the fraction of α -particles falls down to approximately 19%, which is connected with the entering into the range of nonperipheral interactions. Such a change leads to a strong suppression of the processes of diffraction decay of the ^{16}O nucleus and the enhancement of the role of cascade processes. In its turn, as Fig. 5, *a* demonstrates, this gives rise to the growth of the formation probability for multicharged fragments with charges $3 \leq z \leq 7$, mainly sevenfold-charged ones, in the interval $\Delta \approx 0.23 \div 0.28$ GeV/c. Figure 5, *a* also demonstrates that there emerges a weak reduction of the formation probabilities for both ^4He nuclei and multicharged fragments with $3 \leq z \leq 7$ in the interval $\Delta \approx 0.3 \div 0.7$ GeV/c. It is of interest to note that the fraction of α -particles grows in the interval $\Delta \approx 0.7 \div 0.85$ GeV/c, whereas the fraction of multicharged fragments with $3 \leq z \leq 7$ diminishes here, and the fractions of light and eightfold-charged fragments remain constant within the statistical error limits. Negative correlations between the formation probabilities for α -particles and multicharged fragments with $3 \leq z \leq 7$, which are observed experimentally in this interval, can probably be explained on the basis of the conservation law for the baryon charge. In the interval

Table 7. Fractions of light fragments ($A \leq 3$), ^4He nuclei, multicharged fragments with $3 \leq z \leq 7$, and eightfold-charged fragments among all fragments with $1 \leq z \leq 8$ averaged over the interval $\Delta = 0.1 \div 1.25$ GeV/c

Fragment	$\langle W \rangle, \%$	
	Experiment	CFEM calculations
$3 \leq z \leq 8$	100	100
$A \leq 3$	53.5 ± 1.3	59.2 ± 0.9
^4He	19.0 ± 1.6	11.4 ± 0.3
$3 \leq z \leq 7$	21.5 ± 1.4	27.2 ± 0.6
$z = 8$	6.0 ± 0.4	2.2 ± 0.1

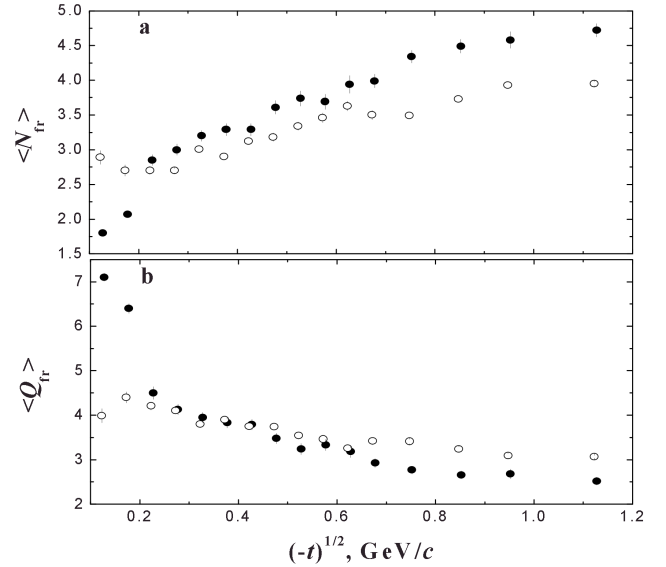


Fig. 6. Dependences of the average number of fragments per event (a) and the average charge of fragments (b) on Δ : experimental data (\bullet) and the results of CFEM calculations (\circ)

$\Delta \approx 0.75 \div 0.95$ GeV/c, the formation probability for α -particles turns out higher than that for the formation of multicharged fragments, while, at $\Delta > 0.95$ GeV/c, the formation probabilities for ^4He nuclei and multicharged fragments with $3 \leq z \leq 7$ become practically identical within the statistical error limits. As is seen from Fig. 5, *a*, the probability of the eightfold-charged fragment formation makes up a plateau in the interval $\Delta > 0.7$ GeV/c and amounts on average to 1.2%. It practically corresponds to the fraction of events, where one or two neutrons are knocked out from an oxygen nucleus without the subsequent destruction of the latter. From Fig. 5, *b*, one can see that the fraction of eightfold-charged fragments also proves constant in the given interval. The results of model calculations, which are exhibited in Fig. 5, *b*, differ strongly from experimental ones. The largest difference is observed in the region of low Δ : the model fails to describe a strong reduction of the fraction of eightfold-charged fragments and the growth of the fractions of light fragments, ^4He nuclei, and multicharged fragments, which is observed in the experiment. The results of model calculations, in contrast to experimental data, do not reveal the region of the change from the peripheral to nonperipheral interactions, which is more clearly illustrated by the comparison between the experimental data and the results of model calculations made in Fig. 6 (panels *a* and *b*). As is seen from Fig. 5 (panels *a* and *b*), the model

considerably underestimates the fraction of eightfold-charged fragments and overestimates the fractions of other fragments at small Δ . At high Δ , the model overestimates the fraction of multicharged fragments with $3 \leq z \leq 7$ and underestimates the fraction of light fragments and α -particles. All that, as is seen from Fig. 6 (panels *a* and *b*), gives rise to the overestimation of the average number of fragments and the underestimation of the average fragment charge at low Δ , as well as to the underestimation of the average number of fragments and the overestimation of the average fragment charge at high Δ . A satisfactory agreement between the model and experimental results is observed, as it becomes evident from Fig. 6, *b*, only for the spectrum of the average charge of fragments and in the intermediate region $\Delta \approx 0.23 \div 0.63$ GeV/*c*. From Table 7, it is seen that the model considerably underestimates, in whole, the average fractions of ${}^4\text{He}$ nuclei and eightfold-charged fragments and overestimates the average fractions of multicharged fragments with $3 \leq z \leq 7$ and light fragments.

3. Conclusions

The main results of this work can be formulated as follows. In whole, the average experimental multiplicities of light ($A \leq 3$) fragments grow, as expected, with increase in Δ . An interesting dependence on Δ is demonstrated by the average multiplicity of ${}^4\text{He}$ nuclei: it increases first; then, within the statistical error limits, it remains constant within the interval $\Delta = 0.3 \div 0.7$ GeV/*c*; and further a weak growth is observed.

The average values of the kinetic energies of fragments with $A = 2$ and 3 , which were measured in the experiment, are practically two or more times larger than those calculated in the framework of the CFEM. Such a discrepancy stems from neglecting – in the model – the contribution of the mechanism of coalescence of fast cascade nucleons leading to the formation of fast few-nucleon fragments. At the same time, the CFEM overestimates the actual average kinetic energy of proton-fragments.

The experimental spectrum of the average kinetic energy of proton-fragments revealed a plateau – not predicted by the theory – in the interval $\Delta > 0.8$ GeV/*c*. This plateau may probably originate from a growth of the average multiplicities of proton-fragments and created π^\pm -mesons in this interval, as well as from the participation of some fraction of fast cascade protons in the formation of fast light fragments through the coalescence mechanism.

Protons constitute the dominant fraction among all light fragments, both in the experiment and in the model. Among all light fragments, the fractions of ${}^1\text{H}$, ${}^2\text{H}$, ${}^3\text{H}$, and ${}^3\text{He}$ nuclei demonstrate the weak dependences on Δ . In contrast to the results of model calculations, the experimental fractions of mirror nuclei ${}^3\text{H}$ and ${}^3\text{He}$ coincide in the whole studied interval of Δ ; this fact evidences for the similarity of physical conditions, under which these nuclei were formed, which may be caused by the charge independence of nuclear forces. The CFEM qualitatively describes the experimental Δ -dependences of the fraction of light fragments, but provides no quantitative agreement. The model overestimates the average fraction of protons and underestimates those of ${}^2\text{H}$ and ${}^3\text{H}$ nuclei; it can be explained by supposing that some portion of fast cascade nucleons with close relative momenta forms fast few-nucleon nuclei through the mechanism of coalescence which is not taken into account by the model under consideration.

The experimental results, in contrast to the calculation ones, clearly reveal a region (in the vicinity of $\Delta \approx 0.23$ GeV/*c*), where the change from the peripheral to nonperipheral ${}^{16}\text{O}$ p-collisions takes place. This region is characterized by the strong growth of the average number of fragments and the strong reduction of their average charge.

The high formation probability for α -particles at peripheral interactions, which is comparable with that for all multicharged fragments with $3 \leq z \leq 7$, as well as the equality – within the statistical error limits – between the average experimental fractions of α -particles and multicharged fragments, evidences for the availability of the α -cluster structure in the oxygen nucleus. At the same time, the model considerably underestimates the actual fraction of α -particles.

The comparison of the experimental data with the results predicted by the CFEM allows one to draw a conclusion that, in order to make an agreement between the model and the experiment better, the model has to take into account the contribution of the coalescence mechanism to the formation of fast few-nucleon fragments, the contributions of diffraction processes at peripheral interactions, and the α -cluster structure of the oxygen nucleus. The data obtained may prove useful for the modification of existing models and the development of new ones dealing with hadron-nucleus collisions at high energies.

To conclude, we would like to express our gratitude to Professor, Dr. Sci. in Physics and Mathematics

V.V. Glagolev who headed the creation of the experimental database on ^{16}O -collisions at 3.25 GeV/c, as well as to the laboratory assistants at the Laboratory of High Energies at the JINR (Dubna, Russia) and the Laboratory of Multiple Processes of the Physical and Technical Institute of the Scientific Production Association "Physics-Sun" of the Uzbek Academy of Sciences (Tashkent, Uzbekistan).

1. W.R. Weber et al., Phys. Rev. C **41**, 520 (1990).
2. L.G. Moretto and G.J. Wozniak, Annu. Rev. Nucl. Part. Sci. **43**, 123 (1993).
3. J.P. Bondorf et al., Phys. Rep. **257**, 133 (1995).
4. A.S. Botvina et al., JINR Commun. P1-90-560 (1990).
5. Yu.P. Yakovlev, Elem. Chast. At. Yadr. **14**, 1093 (1983).
6. E.O. Abdurakhmanov et al., Yad. Fiz. **28**, 1304 (1978).
7. V.A. Karnaukhov et al., Yad. Fiz. **62**, 272 (1999); J. Povlot et al., Phys. Lett. B **233**, 16 (1989).
8. M.A. Belov, K.G. Gulamov, V.V. Lugovoi et al., Yad. Fiz. **65**, 990 (2002); E.Kh. Bazarov, V.V. Glagolev, K.G. Gulamov et al., Yad. Fiz. **67**, 2207 (2004); E.Kh. Bazarov, Yad. Fiz. **69**, 170 (2006).
9. V.V. Glagolev, K.G. Gulamov, V.D. Lipin et al., Yad. Fiz. **63**, 575 (2000); V.V. Glagolev, K.G. Gulamov, M.Yu. Kratenko et al., Yad. Fiz. **58**, 2005 (1995).
10. V.V. Glagolev, K.G. Gulamov, V.D. Lipin et al., Phys. Atom. Nucl. **62**, 1388 (1999).
11. V.V. Glagolev, K.G. Gulamov, V.D. Lipin et al., Eur. Phys. J. A **11**, 285 (2001).
12. E.Kh. Bazarov, V.V. Glagolev, V.V. Lugovoi et al., Pis'ma Zh. Eksp. Teor. Fiz. **81**, 174 (2005).

13. V.V. Glagolev, K.G. Gulamov, M.Yu. Kratenko et al., Pis'ma Zh. Eksp. Teor. Fiz. **58**, 497 (1993).
14. V.V. Glagolev, K.G. Gulamov, M.Yu. Kratenko et al., Pis'ma Zh. Eksp. Teor. Fiz. **59**, 316 (1994).
15. A.S. Botvina et al., Nucl. Phys. A **507**, 649 (1990).
16. F. Butler and C.A. Pearson, Phys. Rev. **129**, 836 (1963).

Received 31.10.06.

Translated from Russian by O.I. Voitenko

ДОСЛІДЖЕННЯ ФРАГМЕНТАЦІЇ ЯДРА КИСНЮ
В ЗАЛЕЖНОСТІ ВІД СТУПЕНЯ ЙОГО
ЗБУДЖЕННЯ У ЗІТКНЕННЯХ
З ПРОТОНАМИ ПРИ
ІМПУЛЬСІ 3,25А ГЕВ/с

*Х.К. Олімов, К. Олімов, С.Л. Лутпуллаєв, А.К. Олімов,
А.А. Юлдашев, Е.І. Ісмаїлов*

Резюме

Наведено нові експериментальні дані, отримані в умовах 4 π -геометрії, із залежностей середніх множинностей легких фрагментів ($A \leq 3$), ядер ^4He , а також середньої кінетичної енергії малонуклонних фрагментів ($A = 1 \div 3$) від величини 4-імпульсу протона-мішені, $\Delta = (-t)^{1/2}$, переданого ядру кисню, в ^{16}O -зіткненнях при імпульсі 3,25А ГеВ/с. Вперше отримано експериментальні дані про залежності імовірності утворення легких фрагментів, ядер ^4He і багатозарядних фрагментів від переданого 4-імпульсу протона-мішені в непружних ^{16}O -зіткненнях. Отримані дані систематично порівнюються з передбаченнями каскадно-фрагментаційної випарювальної моделі.